*International Journal of Latest Research in Engineering and Management" (IJLREM)*
*ISSN: 2456-0766*
*www.ijlrem.org ǁ Volume 05 Issue 03 ǁ March 2021 ǁ PP 19-28*

# Stagnation-Point Flow of a Radiative Tangent Hyperbolic Nanofluid over a Nonlinear Surface with Variable Thermal Conductivity

O. A. Agbolade[1], E. O. Fatunmbi[2]
[1-2]*Department of Mathematics and Statistics, Federal Polytechnic, Ilaro, Nigeria.*

**Abstract:**This study investigates the boundary layer stagnation point flow of hydromagnetic tangent hyperbolic nanofluid over a nonlinear plane in a porous device under the influence of a prescribed power law thermal condition. The modelled partial differential equations outlining the flow problems are translated into ordinary ones using suitable similarity transformation variables. The resultant equations are numerically solved by the shooting technique together with Runge-Kutta Fehlberg scheme. The effects of the various physical parameters are graphically analyzed and deliberated. The obtained results are validated with related existing studies in the limiting position and found to be in perfect agreement. The results indicate that the hydrodynamic boundary layer structure together with velocity profile decelerate when Darcy and magnetic parameters increase whereas the temperature profile appreciates with these terms. Temperature ratio or wall heating parameter triggers a rise in the heat transfer while the thermal field grows with an increase in the magnitude of thermophoresis and Brownian motion terms. Also, the heat transfer at the surface is a decreasing function of these terms.
**Keywords:**Magnetohydrodynamic; Radiation; Porous medium; Tangent hyperbolic nanofluid.

## 1 Introduction

The suspension of nanoparticles in traditional fluids such as water, oil, ethylene glycol, etc is described as nanofluid. This composition is to improve the thermal properties of the fluid and at such the heat transfer capacity of the fluid is enhanced. Also, such a blend offeres unique characteristics often needed in various industrial and engineering operations such as in transportation industries, pharmaceutical processes, cooling of engines and vehicles, etc. Choi and Eastman [1] initialized such a concept which, owing to crucial applications has been widely extended by various authors on Newtonian/non-Newtonian fluids. Abolbashari *et al.* [2] generated results for the transport of Casson nanofluid activated by a stretched sheet coupled with convective wall situation and slip property. Of recent, Alsaedi *et al.* [3] offered an analytical report on such subject with the use of Eyring-Powell nanofluid associated with Ohmic heating and thermophoresis effect. More reports on this concept can be found in Refs [4-6].

The non-Newtonian fluids provide huge engineering and technological applications that makes them a sought-after in the recent years. These wide applications can be found in food processing, oil drilling, pharmaceutical operations, bio-medical engineering, chemical engineering operations and so on. Various branches and mathematical models capturing the non-Newtonian fluids transport exists in the literature due to diverse physical differences in the constitutive relations of fluids. The tangent hyperbolic fluid characterizes shear-thinning properties of non-Newtonian fluid, its concept originated from This model is simple and attractive and its preference over other constitutive non-Newtonian models stems from the fact that its constitutive laws are deduced from the theory of molecular kinetic as against conventional empirical relations. Common examples of fluids that characterize the tangent hyperbolic properties include the biological and industrial fluids (e,g. blood, ketchup, paints, melts solution and polymers). Due to its importance, various researchers have reported such fluids on different geometries. For example, Ullah *et al.* [7] numerically reported the transport of such fluids prompted a stretchable sheet with internal heat source associated with Lie group analysis, Mahdy [8] discussed numerically tangent hyperbolicnanofluid flow configured in a stretchable cylinder with non-uniform temperature whereas Malik *et al.* [9] analyzed such fluids using the same configuration coupled with magnetic field impact and reported that a higher flow resistance occurred with an enlargement of the material parameter and magnetic field term.

Stagnation point flow describes a region of highest static pressure where at the same time the heat transfer and mass deposition attain maximum level whereas the velocity is zero. The applications of such a phenomenon can be encountered in the engineering and industrial operations including the cooling of electronic appliances by fans, thermal oil recovery, the extrusion of polymers in melt-spinning processes and so on. Pioneering such a study, Hiemenz [10] worked on a two-dimensional flat sheet. Afridi *et al.* [11] conducted an analysis on such phenomenon engaging a Newtonian fluid enclosed in a stretchable sheet with Ohmic heating and entropy generation. Animasaun [12], Fatunmbi and Adeniyan [13] engaged micropolar fluid to investigate such a concept on a steady stretchable sheet with an internal heat source.

In many engineering processes and material manufacturing which require high temperature (e.g Nuclear power plants, hot rolling, heat exchangers, electrical power generation), the knowledge of thermal radiation is important for the construction of relevant devices. Generally, the radiative heat flux can be modelled as linear or nonlinear types depending on the magnitude of temperature difference that exists within the flow. The linear type is operative in the case of low temperature difference whereas the nonlinear type is relevant for the situations of low and high temperature differences. Of recent, Al-Khaled *et al.* [14] conducted research showing the significance of such a concept in the transport of a reactive tangent hyperbolic fluid while Khan *et al.* [15] using the same fluid to study the impact of nonlinear radiation associated with an internal heat source in the neighborhood of a stagnation region. For wider applications of thermal radiation, the present study has incorporated the general nonlinear thermal radiation model [16-18].

The present study aims to carry out an investigation on the stagnation point flow in hydromagnetic tangent hyperbolic nanofluid towards over a nonlinear stretching sheet in a porous enclosure under the influence of variable thermal conductivity. The consequential applications of such study have motivatated its analysis. More so, the study incorporates the influence of nonlinear thermal radiation, prescribed surface temperature and concentration boundary conditions.

## 2 Problem Development and Governing Equations

Consider a steady, two dimensional, incompressible and stagnation point flow of hydromagnetic tangent hyperbolic nanofluid over an impermeable and nonlinearly stretching sheet with the influence of temperature-dependent thermal conductivity. The coordinate system is taken to be $(x, y)$ with the respective velocity components indicated as $(u, v)$ where $x$ axis signifies the flow direction with normal axis being $y$ as shown in Fig. 1. The nonlinear stretching sheet has the velocity $u = U_s = hx^{\alpha}$ whereas the velocity at the upstream is $u = U_b = qx^{\alpha}$ where $h > 0, q$ and $\alpha$ are the stretching parameter, a constant which measures stagnation point flow potency and the nonlinear stretching term related to the surface stretching speed in that order. The magnetic field is imposed normal to the flow direction and it is taken as $B(x) = B_0 x^{(\alpha-1)/2}$. In the energy equation, the heat transfer is being influenced by Joule heating, viscous dissipation, nonlinear thermal radiation as well as thermophoresis and Brownian motion. Note that $MBL, TBL$ and $CBL$ in Fig. 1 respectively describe the Momentum boundary layer, Thermal boundary layer and Concentration boundary layers.

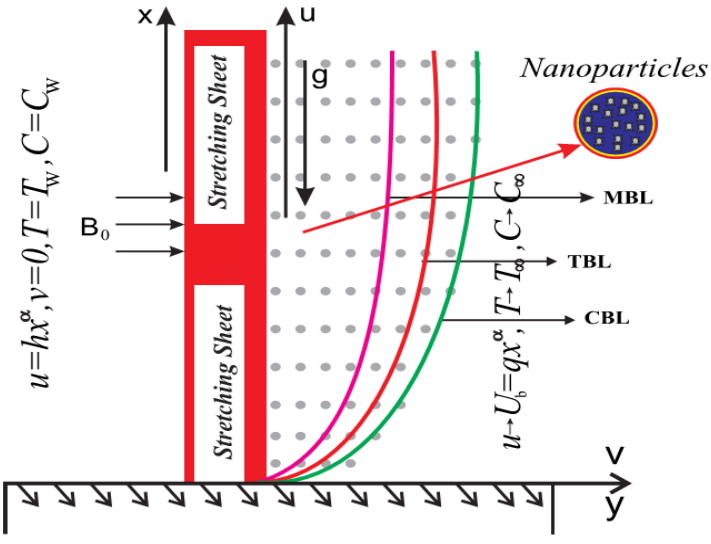


**Fig. 1** The Flow Configuration

Incorporating these assumptions together with the principles of the boundary layer approximations, the following equations are the formulated boundary layer equations for the hydromagnetic tangent hyperbolic nanofluid.

$$\frac{\partial u}{\partial x}+\frac{\partial v}{\partial y}=0, \tag{1}$$

$$\left(u\frac{\partial u}{\partial x}+v\frac{\partial u}{\partial y}\right)=U_b\frac{dU_b}{dx}+\frac{\mu_f}{\rho_f}(1-\beta)\frac{\partial^2 u}{\partial y^2}+\frac{\mu_f}{\rho_f}\sqrt{2}\kappa\Gamma\frac{\partial^2 u}{\partial y^2}\frac{\partial u}{\partial y}-\frac{\sigma B(x)^2}{\rho}(u-U_b)-\frac{\mu_f}{\rho_f K_p}(u-U_b), \tag{2}$$

$$(\rho c_p)_f\left(u\frac{\partial T}{\partial x}+v\frac{\partial T}{\partial y}\right)=\frac{\partial}{\partial y}\left(k\frac{\partial T}{\partial y}\right)+(\rho c_p)_p\left(\frac{\partial T}{\partial y}\right)\left[\frac{D_T}{T_\infty}\left(\frac{\partial T}{\partial y}\right)+D_B\left(\frac{\partial C}{\partial y}\right)\right]+\sigma B(x)^2(u-U_b)^2+\frac{\mu_f}{K_P}(u-U_b)^2+\frac{16\zeta^{\text{å}}}{3a^{\text{å}}}\frac{\partial}{\partial y}\left(T^3\frac{\partial T}{\partial y}\right), \tag{3}$$

$$u\frac{\partial C}{\partial x}+v\frac{\partial C}{\partial y}=D_B\frac{\partial C^2}{\partial y^2}+\frac{D_T}{T_\infty}\left(\frac{\partial^2 T}{\partial y^2}\right). \tag{4}$$

The accompanied boundary conditions for equations (5-8) are:

$$u=U_s=hx^\alpha, v=0, T=T_w\left(=T_\infty+Bx^{m_1}\right), C=C_w\left(=C_\infty+Dx^{m_2}\right)\ when\ y=0,$$
$$u\to U_b=qx^\alpha, T\to T_\infty, C\to C_\infty,\ \ with\ \ y\to\infty. \tag{5}$$

The expression for the thermal conductivity as relates to temperature is presented as,

$$k=\frac{k_\infty}{T_w-T_\infty}\left[(T_w-T_\infty)+\delta(T-T_\infty)\right]. \tag{6}$$

with $k_\infty$ being the constant thermal conductivity while $\delta$ defines the thermal conductivity parameter. Similarly, the permeability of the porous medium in Eq. (6) is indicated as $K_p=K_0x^{1-\alpha}$, where $K_0$ is a constant. The underlisted dimensionless variables are introduced into the main equations [19-20].

$$\eta=\sqrt{\frac{h(\alpha+1)x^{\alpha-1}}{2\nu}}y, \psi=\sqrt{\frac{2\nu hx^{\alpha+1}}{\alpha+1}}f(\eta), \theta(\eta)=\frac{T-T_\infty}{T_w-T_\infty}, Nr=\frac{16\zeta^{\text{å}}T_\infty^3}{3a^{\text{å}}k_\infty}, Re=\frac{U_s x}{\nu_f}$$
$$\phi(\eta)=\frac{C-C_\infty}{C_w-C_\infty}, u=\frac{\partial\psi}{\partial y}, v=-\frac{\partial\psi}{\partial x}, Nt=\frac{(\rho c_p)_p D_T\left(T_w-T_\infty\right)}{(\rho c_p\nu)_f T_\infty}, H=\frac{q}{h}, Da=\frac{\nu}{hK_0}$$
$$\theta_w=\frac{T_w}{T_\infty}, Pr=\frac{\mu_f c_p}{k_\infty}, M=\frac{\sigma B_0^2}{h\rho}, Sc=\frac{\nu}{D_B}, We=\Gamma\sqrt{\frac{h^3x^{3r-1}(\alpha+1)}{\nu_f}}, Ec=\frac{U_w^2}{C_p(T_w-T_\infty)}$$
$$Nb=\frac{(\rho c_p)_p D_B\left(C_w-C_\infty\right)}{(\rho c_p\nu)_f}. \tag{7}$$

The substitution of quantities in (12) into the governing Eqs. (5-8) yields:

$$\left((1-\beta)+\beta We f''\right)f'''+ff''-\frac{2\alpha}{\alpha+1}\left(f'^2-A^2\right)-\frac{2}{\alpha+1}\left(M+Da\right)\left(f'-A\right)=0, \tag{8}$$

$$\left[1+\delta\theta+Nr\left(1+(\theta_w-1)\theta\right)^3\right]\theta''+3Nr\left(\theta_w-1\right)\theta'^2\left(1+(\theta_w-1)\theta\right)^2+Pr\left(f\theta'-\frac{2m_1}{\alpha+1}f'\theta\right)+$$
$$Pr\left(N_t\theta'^2+N_b\theta'\phi'\right)+\frac{2}{\alpha+1}\left(M+Da\right)\left(f'-H\right)^2Pr+\delta\theta'^2=0, \tag{9}$$

$$\phi''+\frac{N_t}{N_b}\theta''+Sc\left(f\phi'-\frac{2m_2}{\alpha+1}f'\phi\right)=0. \tag{10}$$

The boundary situations transform to:

$$f'(0)=1,\ f(0)=0, 0(0)=1, \phi(0)=1.$$
$$f'(\infty)=A, \theta(\infty)=0, \phi(\infty)=0. \tag{11}$$

**Table 1**: Description of the Symbols

| Symbols | Description | Symbols | Description |
|---|---|---|---|
| $C$ | Concentration | $Nb$ | Brownian motion parameter |
| $C_w$ | Concentration at the sheet | $a*$ | Mean absorption coefficient |
| $C_\infty$ | Concentration at the free stream | $Nt$ | Thermophoretic parameter |
| $Da$ | Darcy parameter | $Pr$ | Prandtl number |
| $D_B$ | Brownian diffusion coefficient | $D_T$ | Thermophoretic diffusion coefficient |
| $Ec$ | Eckert number | $Sc$ | Schmidt number |
| $T_w$ | Temperature at the sheet | $T$ | Temperature |
| $u$ | Velocity in $x$ direction | $T_\infty$ | Temperature at free stream |
| $H$ | Velocity ratio parameter | $U_s$ | Velocity at the sheet |
| $K_1^2$ | Chemical reaction rate | $v$ | Velocity in $y$ direction |
| $M$ | Magnetic field term | $We$ | Weissenberg number |
| | Temperature exponent | $x, y$ | Cartesian coordinates |
| Greek letters | **Description** | Greek letters | **Description** |
| $\mu_f$ | Base fluid viscosity | $\rho_f$ | Base fluid density |
| $\gamma_1$ | Chemical reaction | $\grave{o}$ | Temperature relative parameter |
| $\nu_f$ | Kinematic viscosity | $\kappa$ | Power law exponent |
| $\theta$ | Dimensionless temperature | $\theta$ | Dimensionless temperature |
| $\theta_w$ | Temperature ratio term | $\theta_w$ | Temperature ratio term |
| $\zeta^{\text{å}}$ | Stefan-Boltzmann constant | $\Gamma$ | Relaxation time |
| $\sigma$ | Electrical conductivity | $(\rho c_p)_f$ | Effective heat capacity of fluid |
| $m_2$ | Concentration exponent | $(\rho c_p)_p$ | Effective heat capacity of nanoparticles |

The quantities of interest for the engineers are the coefficient of skin friction $C_{fx}$, the Nusselt number $Nu_x$ and the Sherwood number $Sh_x$. These quantities are orderly presented as follows.

$$C_{fx}=\frac{2\tau_w}{\rho_\infty U_s^2}, Nu_x=\frac{xq_w}{k_\infty\left(T_w-T_\infty\right)}, Sh_x=\frac{xq_m}{D_B\left(C_w-C_\infty\right)}, \tag{12}$$

$$\tau_w = \mu_\infty \left[ \frac{\partial u}{\partial y} + \frac{\Gamma}{\sqrt{2}} \left( \frac{\partial u}{\partial y} \right)^2 \right]_{y=0}, q_w = -\left[ \left( k_\infty + \frac{16T^3\sigma^{å}}{3k^{å}} \right) \frac{\partial T}{\partial y} \right]_{y=0}, q_m = -\left( D_B \frac{\partial C}{\partial y} \right)_{y=0}, \quad (13)$$

where $\tau_w$ indicates surface shear stress, $q_w$ represents surface heat flux and $q_m$ denotes the surface mass flux in that order. Using Eqs. (12) and (18), the dimensionless $C_{fx}$ is written in Eq. (19) while that of $Nu_x$ and $Sh_x$ are respectively presented in Eq. (20).

$$Re_x^{\frac{1}{2}} C_{fx} = 2(\alpha+1)^{\frac{1}{2}} \left[ (1+\beta) f''(0) + \frac{We}{2} f''^2(0) \right], \quad (14)$$

$$Re_x^{-\frac{1}{2}} Nu_x = -\left( \frac{\alpha+1}{2} \right)^{\frac{1}{2}} \left[ 1 + Nr\left(1 + (\theta_w - 1)\theta(0)\right)^3 \right] \theta'(0), Re_x^{-\frac{1}{2}} Sh_x = -\left( \frac{\alpha+1}{2} \right)^{\frac{1}{2}} \phi'(0). \quad (15)$$

## 3 Numerical Method with validation

The system (13) to (15) subject to (16) depicts a boundary value problem with high degree of nonlinearity, thus, an exact solution to the system seems difficult to asses. In this view, an approximate numerical solution is sought by a famous shooting technique coupled with Runge-Kutta-Fehlberg method. Based on the popularity of this method as described and applied by many authors ([21-24]), we do not give its details here. We set $\beta = We = \zeta_1 = \zeta_2 = N_t = N_b = m_1 = m_2 = 0.1, \theta_w = 1.3, Q = 0.01,$ $Da = M = \delta = Nr = \lambda_1 = \lambda_2 = G = r = N = 0.2, Sc = \alpha = 1.0$ and $Pr = 2.0$ as parametric values unless listed otherwise in the plots. To crosscheck the credibility of the results obtained in the current study, a comparative analysis of $f''(0)$ for variations in $M$ with previously reported data of Mabood and Das [22] and Xu & Lee [23] is reported in Table 2 and a comparative study of $(-\theta(0))$ for different $Pr$ with previously published results of Ali [24] alongside with Mabood and Shateyi [25] is recorded in Table 3 which validate our code. The comparisons of solutions are shown in Table 2 and 3, reasonable agreement is obtained with earlier computations which confirm the validity of the present numerical solutions.

**Table 2:** Values of $f''(0)$ in comparison with [22-23] as $M$ changes when $\beta = We = H = Da = \lambda_1 = \lambda_2 = N = 0, Pr = \alpha = 1.0$.

| $M$ | [22] | [23] | Present Study |
|---|---|---|---|
| 0 | 1.000008 | - - | 1.00000 |
| | -1.4142135 | -1.41421 | -1.41421 |
| | -2.4494987 | -2.4494 | -2.44949 |
| | -3.3166247 | -3.3166 | -3.31662 |
| | -7.1414284 | -7.1414 | -7.14143 |
| | -10.049875 | -10.0498 | -10.04989 |
| | -22.383029 | -22.3830 | -22.38302 |
| | -31.638584 | - | -31.63863 |

**Table 3:** Comparism of values $(-\theta'(0))$ with [24] and [25] for changess in $Pr$ when $m_1 = m_2 = \alpha = 1.0$ and $\delta = Nr = Ec = Q = G = M = H = Da = 0$.

| $Pr$ | **[24]** | **[25]** | **Present Study** |
|---|---|---|---|
| 0.72 | 0.8058 | 0.8088 | 0.808637 |
| .0 | 0.9691 | 1.0000 | 1.000000 |
| .0 | 1.9144 | 1.9237 | 1.923683 |
| .0 | 3.7006 | 3.7207 | 3.720674 |

## 4 Presentation of Results

The physical impacts of the selected parameters on the various dimensionless quantities are presented graphically (Figures 2-14) and discussed in this section. The plot capturing the reactions of the velocity field versus $\eta$ is presented in Figs. 2. In clear terms, there is a decelerated flow as the magnetic field ( $M$ ) parameter enlarges. Such a trend is induced by the action of the Lorentz force occasioned by the interaction of the transversely applied magnetic field and the electrically conducting tangent hyperbolic fluid.

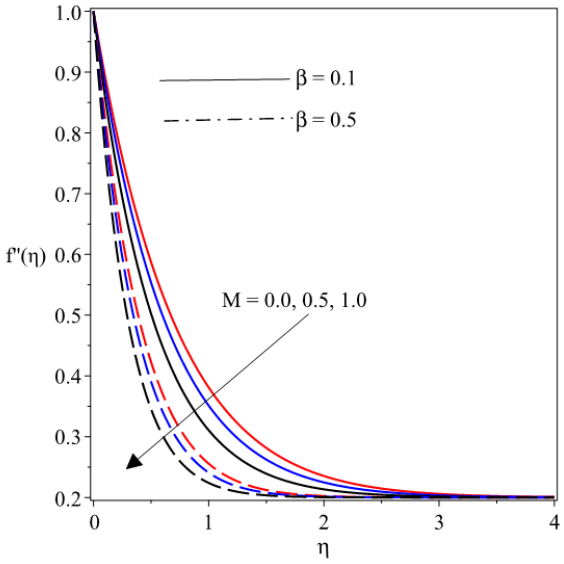


**Fig. 2** Plots of velocity distribution with variations in $M\&\beta$

Hence, a hike in $M$ improves the Lorentz force and consequently compel a reduction in the flow regime. The power law exponent $\beta$ in the presence of M also reduces the flow and has a diminishing influence on the velocity regime as depicted in Fig. 2. This pattern resulted from an enhanced strength of viscosity as the magnitude of $\beta$ enlarges. Figure 3 informs that the increasing trend in $M$ raises the temperaturein the presence of $\beta$. This can be attributed to the additional friction created in the flow field as a result of Lorentz force due to magntic field influence. Similarly, an increase in $\beta$ created an expansion in the thermal boundary layer and consequntly compel the temperature to increase as shown in Fig. 3.

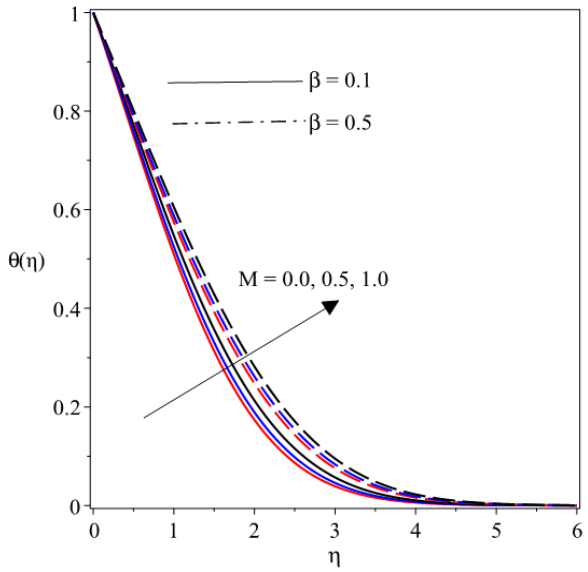


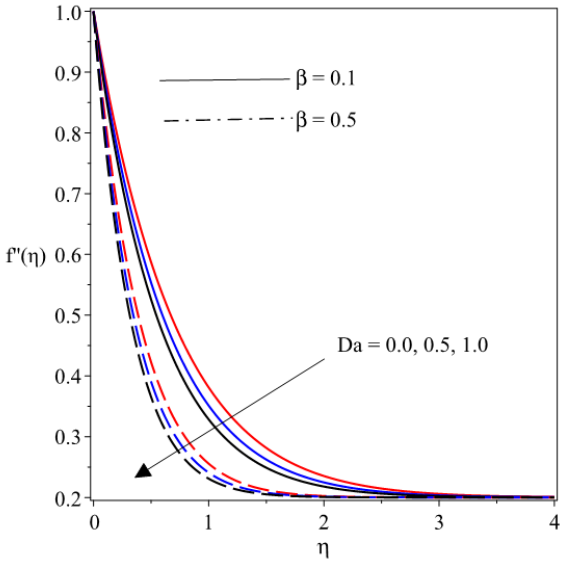


**Fig. 3** Temperature distribution $M$ & $\beta$ **Fig. 4** Velocity profiles for variations in $Da$ & $\beta$

Figure 4 reveals that the fluid motion decreases with rising values of the Darcy number $Da$ in the existence of $\beta$. An increase in $Da$ creates a resistance for the fluid flow as noticed in this figure. It is observed

that the fluid flow is higher for non-porous medium, that is, $Da = 0$ than for porous medium ($Da \neq 0$). Contrarily, the temperature field is enhanced as $Da$ is increasing in magnitude as clearly shown in Figure 5. This is due to the thickness of the thermal boundary layer for growth in $Da$.

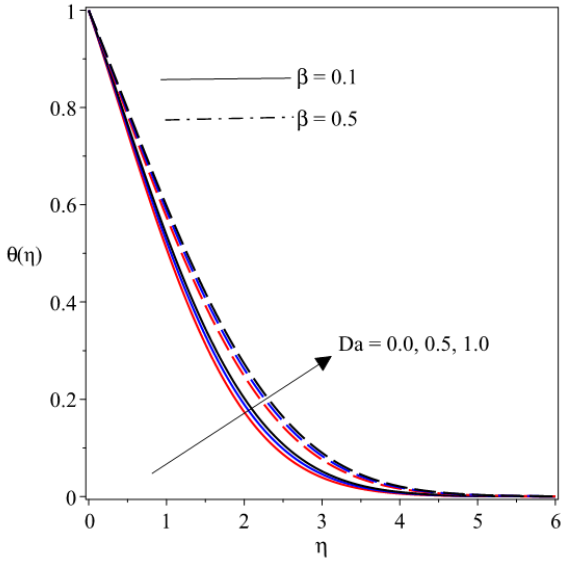


**Fig. 5**Temp. verus $\eta$ for variation in $Da\&\beta$

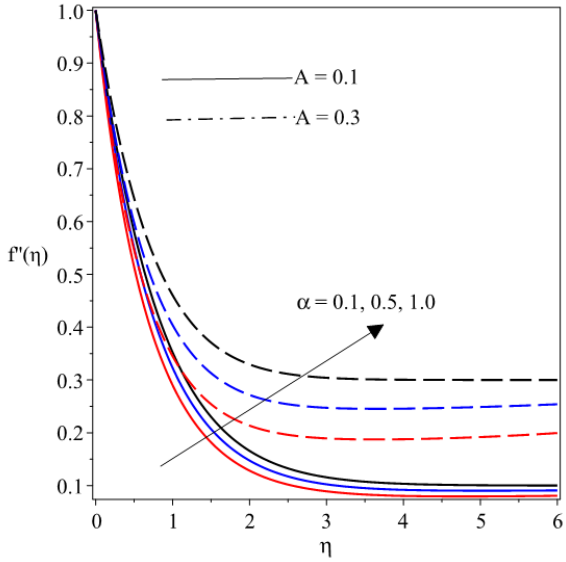


**Fig. 6** Velocity field for varying$A\&\alpha$

The nonlinear stretching parameter $\alpha$ and the velocity ratio parameter boost the momentum boundary layer thickness and thus accelerate the motion of the fluid as demonstrated in Fig. 6. The upstream velocity is moving faster than the sheet velocity, hence the reduction in the drag and accelerate flow is recorded due a hike in the velocity ratio term.

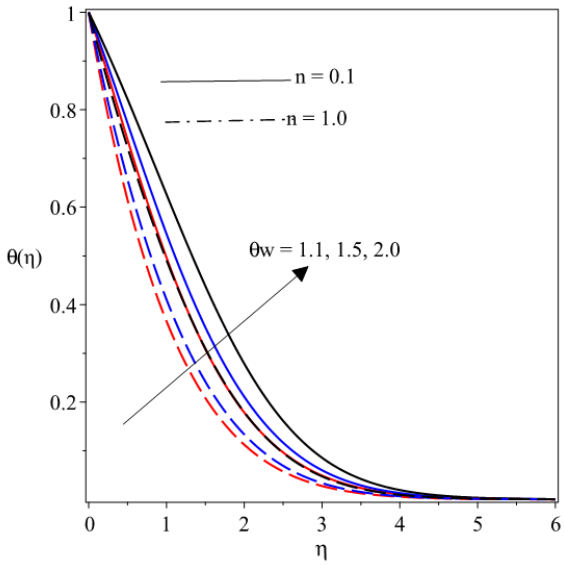


**Fig. 7** Temp field for variation in $\theta w\&n$

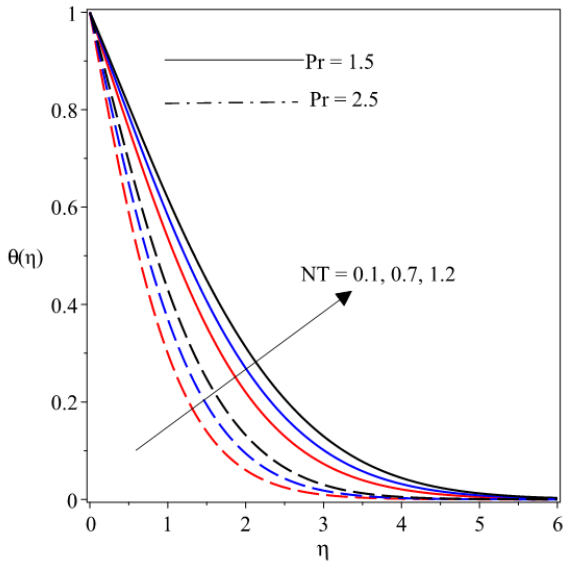


**Fig. 8** Tempfield for different values of $NT\&Pr$

Figure 7 portrays the impact of the temperature parameter and the temperature exponent term on the surface temperature. Here, it is seen that the thermal boundary layer is energized due to a rise in $\theta w$ whereas the temperature exponent term $n$ diminishes the thermal boundary layer and consequently lowers the average temperature. Similarly, a rise in $\theta w$ connotes a higher sheet temperature as compared to the upsream temperature, hence, the surface temperature rises.

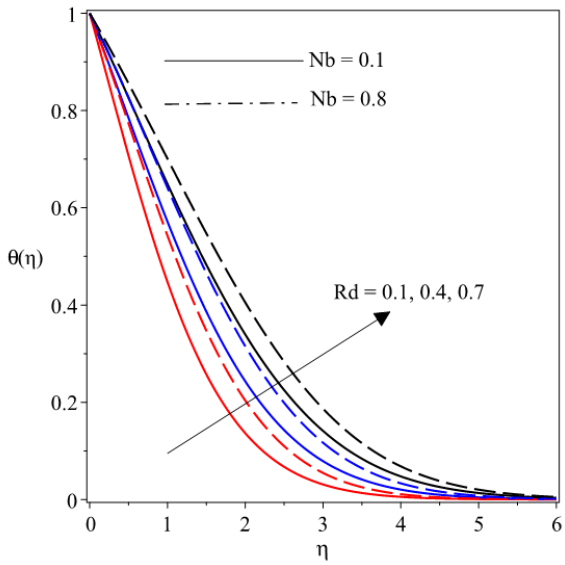


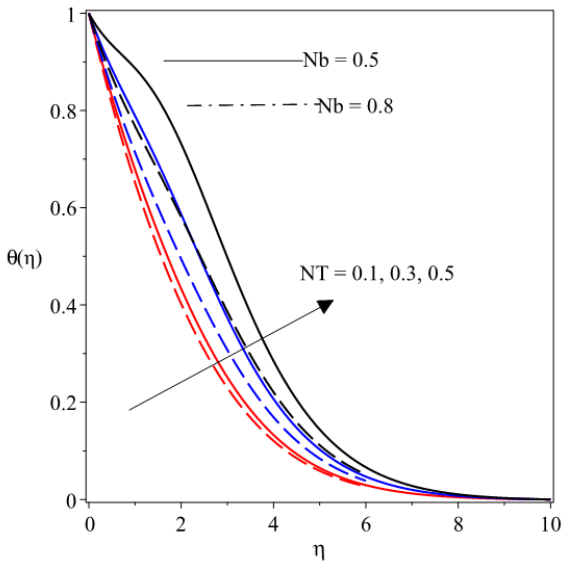


**Fig. 9** Temp field for variation in $Rd\&Nb$ **Fig. 10**Tempfield for different values of $NT\&Nb$

Figure 9 depicts the influence of radiation parameter and Brownian motion term on the temperature profiles. A rise in the magnitude of $Rd$ enhances the surface temperature as clearly shown in this figure. Similarly, haphazard motion of tiny particles compels a thicken boundary layer structure and thereby boost the temperature profiles as described in Fig. 9. In the same vein, the influence of the thermophoresis parameter is to cause a thickness in the thermal boundary structure which in turn boost the temperature across the boundary layer as clearly displayed in Fig. 10.

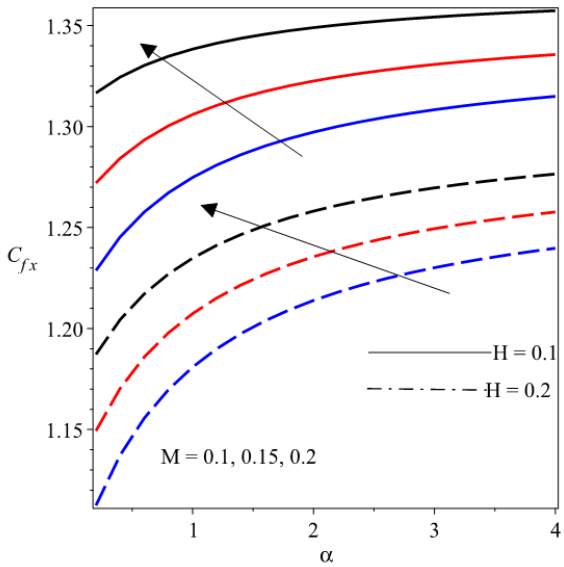


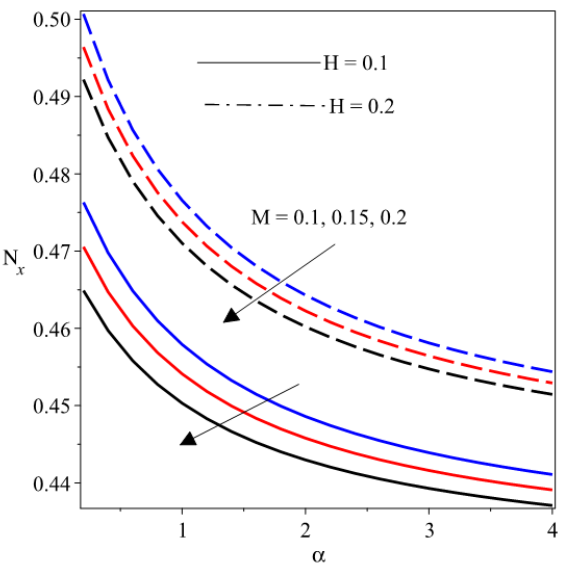


**Fig. 11**Combinedeffcets of $M$ & $H$ on $C_{fx}$ **Fig. 12** Combined effcets of $M$ & $H$ on $N_{ux}$

In Fig. 11, an increase in $M$ promotes a higher skin friction coefficient. In this case, the drag phenomenon is increased to higher magnitudes of $M$ whereas a rise in the stretching parameter $H$ lowers the skin friction coefficient $C_{fx}$ as showcased in Fig. 11. On the contrary, the heat transfer denoted as the Nusselt number $N_{ux}$ depreciates with a hike in $M$ while it accelerates with a boost in $H$ as shown in Fig. 12.

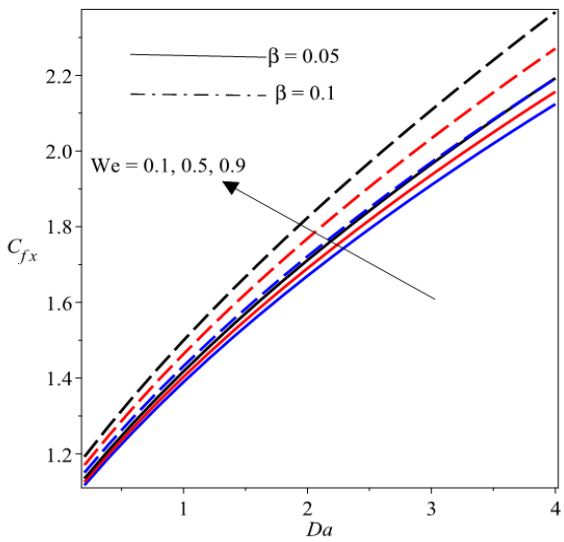


**Fig. 13**Combined effcets of $We\&\beta$ on $C_{fx}$

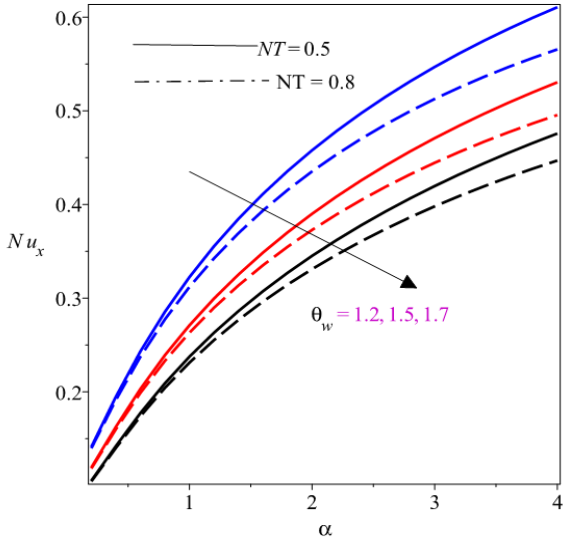


**Fig. 14**Combined effcets of $\theta w\&NT$ on $N_{ux}$

A rise in the Weisseiberg number $We$ cause the skin friction coefficient to be increased whereas the opposite is the case for higher $\beta$ as depicted in Fig. 13. This means that an increment in the strength of Weissenberg number ( $We$ ) with the power law exponent accelerates the coefficient of skin friction as demonstrated in Fig. 13. In Fig. 14, both $\theta w$ and $NT$ act to reduce the rate of heat transfer across the surface of the sheet.

## 5 Conclusion

A physical model is developed for the thermo-solutal transport of a tangent hyperbolic nanofluid in the neighbourhood of a stagnation point from a nonlinear stretchable sheet enclosed in a porous device. Also included in the model are the impacts of nonlinear thermal radiation and activation energy with MHD. The transformed dimensionless nonlinear boundary value problem has been solved with the Runge-Kutta Fehlberg coupling shooting technique. Validation with previous studies reveals perfect correlation in the limiting cases. A parametric study of the impact of selected variables on the transport characteristics has been constructed graphically. The simulations have shown that:

- Increment in the Darcy $Da$, power law exponent $\beta$ and magnetic field $M$ terms lead to the diminution of the flow field.
- Rise in the velocity ratio term $H$ upsurges fluid velocity while that peters out the temperature.
- There is an improvement in the tangent hyperbolic fluid temperature with the increased values of the radiation $Nr$, heat source $Q$, thermophoresis $N_t$ and Eckert number $Ec$ parameters.
- Skin friction coefficient is strengthened due to higher magnetic $M$, power law exponent $\beta$ and Darcy parameters $Da$ while a reversed trend occurred with a rise in $H$.
- Nusselt number appreciates in respect of the Prandtl number $Pr$, temperature ratio term $\theta_w$ and $Nr$ while the opposite is the case for $N_t$, $N_b$ and $Ec$.
- The mass transfer enlarges for incremental values of $Da, M$ whereas it falls with thermophoresis term $NT$

## References

[1]. Choi, S. U. S. and Eastman J. A. Enhancing thermal conductivity of fluids with nanoparticles (No. ANL/MSD/CP-84938; CONF-951135-29), Argonne National Lab., IL (United States), (1995).

[2]. Abolbashari, H. M, Fredoonimehr, N., Nazari, F. and Rashidi, M. M. Analytical modelling of entropy generation for Casson nano-fluid flow induced by a stretching sheet, Advanced Powder Technology, 1-12 (2015), http://dx.doi.org/10.1016/j.apt.2015.01.003

[3]. Alsaedi, A. Hayat, T., Qayyum, S. and Yaqoob, R. Eyring-Powell nanofluid flow with nonlinear mixed convection:Entropy generation minimization, Computer Methods and Programs in Biomedicine, 186, 1-9 (2020).

[4]. Fatunmbi, E. O. and Adeosun, A. T.(2020).Nonlinear radiative Eyring-Powell nanofluid flow along a vertical Riga plate with exponential varying viscosity and chemical reaction. International Communications in Heat and Mass Transfer 119 (2020) 104913.

[5]. Hafeez, A., Khan, M., Ahmed, A and Ahmed, J. Rotational flow of Oldroyd-B nanofluid subject to Cattaneo-Christov double diffusion theory. Appl. Math. Mech. -Engl. Ed. Applied Mathematics and Mechanics (English Edition) (2020) https://doi.org/10.1007/s10483-020-2629-9

[6]. Akbar, N. S., Nadeem, S., Haq, R. U. and Khan. Radiation effects on MHD stagnation point flow of nano fluid towards a stretching surface with convective boundary condition. *Chinese Journal of Aeronautics*, **26**(6), 1389-1397 (2013)

[7]. Ullah, Z. and Zaman, G. Lie group analysis of magnetohydrodynamic tangent hyperbolic fluid flow towards a stretching sheet with slip conditions, Heliyon 3, 1-15 (2017) e00443. doi: 10.1016/j.heliyon.2017.e00443

[8]. Mahdy, A. Entropy generation of tangent hyperbolic nanofluid flow past a stretched permeable cylinder: Variable wall temperature, Process Mechanical Engineering, 0(0), 1ï¿½11 (2018).

[9]. Malik, M. Y., Salahuddin, T. and Hussain, A. and Bilal, S. MHD flow of tangent hyperbolic fluid over a stretching cylinder: Using Keller box method, Journal of Magnetism and Magnetic Materials 395, 271ï¿½276 (2015).

[10]. Hiemenz, K. Die Grenzschicht an einem in den gleich for mingen flussigkeits strom eigetauchten graden Kreiszylinder, Dingerls Polytech. J., 326, 321-324 (1911).

[11]. Afridi, M. I., Qasim, M., Khan, I., Tlili, I. Entropy generation in MHD mixed convection stagnation-point flow in the presence of joule and frictional, Case Studies in Thermal Engineering heating, 12, 292-300 (2018).

[12]. Animasaun, I. L. Melting heat and mass transfer in stagnation point micropolar fluid flow of temperature dependent fluid viscosity and thermal conductivity at constant vortex viscosity, Journal of the Egyptian Mathematical Society, 25, 79ï¿½85 (2017).

[13]. Fatunmbi, E. O. and Adeniyan, A. MHD stagnation point-flow of micropolar fluids past a permeable stretching plate in porous media with thermal radiation, chemical reaction and viscous Dissipation, Journal of Advances in Mathematics and Computer Science, 26(1), 1-19 (2018).

[14]. Al-Khaled, K., Khan, S. U. and Khan, I. Chemically reactive bioconvection flow of tangent hyperbolic nanoliquid with gyrotactic microorganisms and nonlinear thermal radiation, Heliyon, 6, 1-7 (2020).

[15]. Khan, M. I, Khan, T. A., Qayyum, S., Hayat, T, Khan, M. I. and Alsaedi, A. Entropy generation optimization and activation energy in nonlinear mixed convection flow of a tangent hyperbolic nanofluid, Eur. Phys. J. Plus, 133, 1-20 (2018).

[16]. Mabood, F., Imtiaz, M, Alsaedi, A. and Hayat, T. Unsteady Convective Boundary Layer Flow of Maxwell Fluid with Nonlinear Thermal Radiation: A Numerical Study, IJNSNS, 17(5), 221ï¿½229 (2016).

[17]. Gbadeyan, J. A., Titiloye, E. O. and Adeosun, A. T. Effect of variable thermal conductivity and viscosity on Casson nanofluid flow with convective heating and velocity slip, Heliyon 6, 1-10 (2020).

[18]. Fatunmbi, E. O. and Adeniyan, A. Nonlinear thermal radiation and entropy generation on steady flow of magneto-micropolar fluid passing a stretchable sheet with variable properties, Results in Engineering, 6, 1-10 (2020).

[19]. Waqas, M., Farooq, M., Khan, M. J., Alsaedi, A., Hayat, T. and Yasmeen, T. Magnetohydrodynamic (MHD) mixed convection flow of micropolar liquid due to nonlinear stretched sheet with convective condition, International Journal of Heat and Mass Transfer, 102, 766-772 (2016).

[20]. Fatunmbi, E. O., Okoya, S. S. and Makinde, O. D. Convective heat transfer analysis of hydromagnetic micropolar fluid flow past an inclined nonlinear stretching sheet with variable thermoï¿½physical properties, Diffusion Foundations, 26, 63-77 (2020).

[21]. Attili, B. S. and Syam, M. L. Efficient shooting method for solving two point boundary value problems, Chaos, Solitons and Fractals, 35(5), 895ï¿½903, (2008).

[22]. Mabood, F. and Das, K. Melting heat transfer on hydromagnetic flow of a nanofluid over a stretching sheet with radiation and second order slip, Eur. Phys. J. Plus 131(3) (2016).

[23]. Xu, L. and Lee, E.W.M. Variational iteration method for the magnetohydrodynamic flow over a nonlinear stretching sheet. Abst Appl Anal 5 pages (2013).

[24]. Ali, M. E. Heat transfer characteristics of a continuous stretching surface,ï¿½ Wï¿½arme-und Stoffï¿½ubertragung, 29(4), 227ï¿½234 (1994).

[25]. Mabood, F. and Shateyi, S. Multiple Slip Effects on MHD Unsteady Flow Heat and Mass Transfer Impinging on Permeable Stretching Sheet with Radiation, Modelling and Simulation in Engineering Volume 2019, Article ID 3052790, 11 pages.